Geoscientific Model Development

Supporting Information for

Improving Shortwave Radiative Transfer in the Lake Component of the Common Land Model (CoLM-Lake) with a Spectral Scheme for the Full Snow-Ice-Water Column

Xueqi Cao[1], Nan Wei[1*], Hua Yuan[1], Shupeng Zhang[1], Zhongwang Wei[1], Xingjie Lu[1], Lu Li[1], and Yongjiu Dai[1]

[1] School of Atmospheric Sciences, Sun Yat-sen University, Zhuhai 519082, China;

Corresponding author: Nan Wei (wein6@mail.sysu.edu.cn)

Contents of this file

Figures S1 to S12
Tables S1 to S3

Introduction

This supporting information provides additional model evaluation and sensitivity analyses for the spectral snow–ice–water radiative-transfer scheme implemented in the lake component of the Common Land Model (CoLM-Lake). It includes twelve supplementary figures and three tables. The figures document lake-specific differences in column-integrated absorbed direct and diffuse shortwave radiation between CoLM-Snicar and CoLM-Extinct, comparisons between observed and simulated lake temperatures at multiple depths and vertical profiles, and sensitivity experiments for vertical mixing and SNICAR-ADv5 input parameters. The tables summarize the spectral optical properties of light-absorbing aerosols in the snowpack used by the radiative transfer calculations, including single scattering albedo, mass extinction coefficient, and asymmetry factor for five shortwave bands.

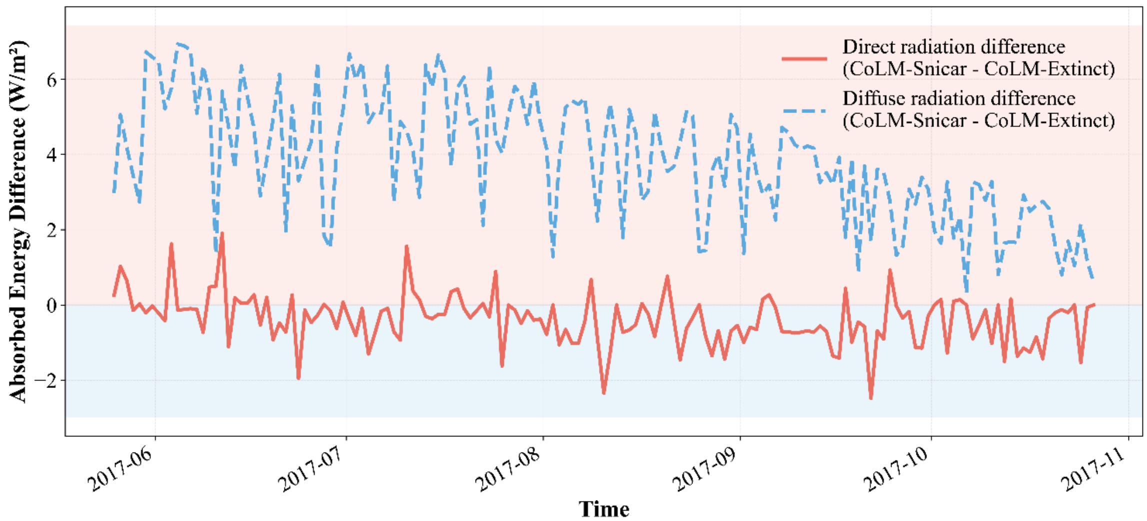

Figure S1. Differences in column-integrated absorbed direct and diffuse shortwave radiation between CoLM-Snicar and CoLM-Extinct during the open-water season of 2017 in Crystal Bog. Positive values indicate larger absorption in CoLM-Snicar.

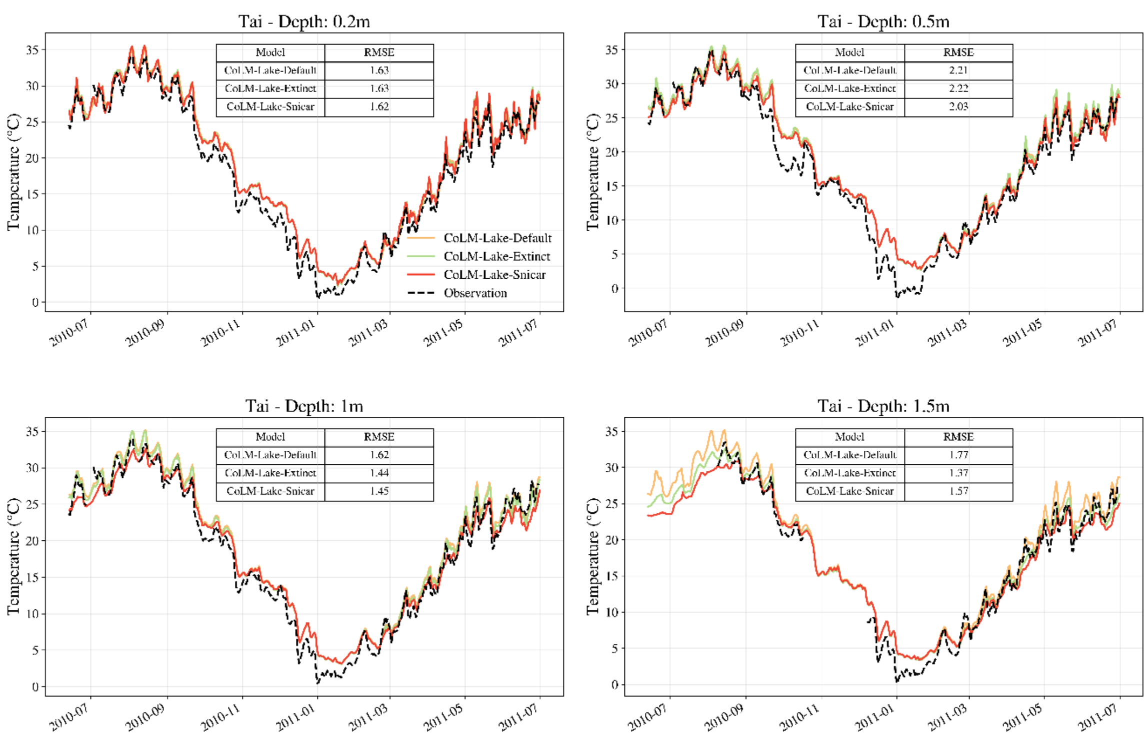

Figure S2. Observed and simulated water temperatures in Lake Tai at four measurement depths under the three model configurations. The inset tables report RMSE values (°C) for each simulation.

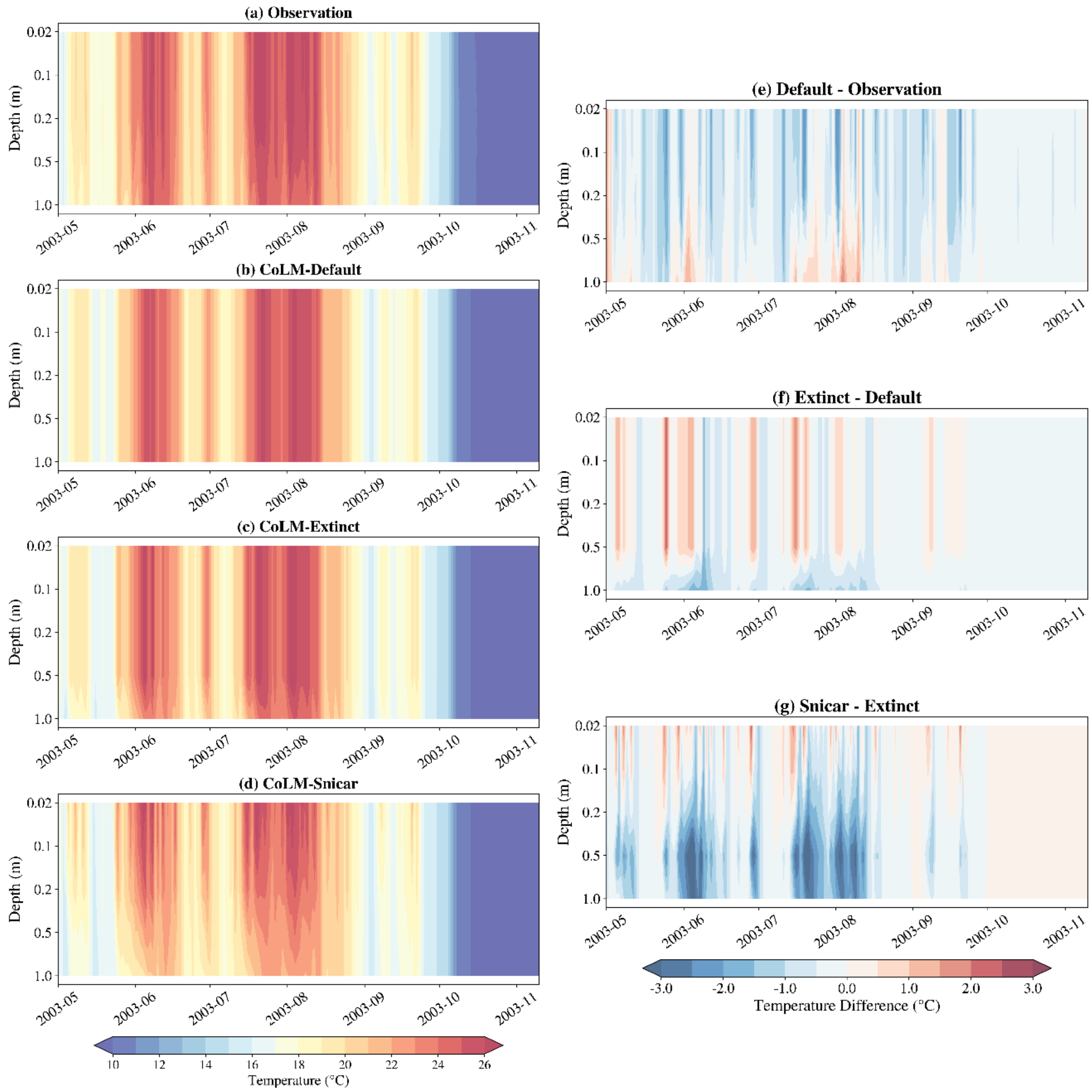

Figure S3. Observed and simulated water-temperature profiles in Lake Kossenblatter. (a) Observations; (b-d) simulations from CoLM-Default, CoLM-Extinct, and CoLM-Snicar, respectively; (e-g) Simulated differences between CoLM-Default and observations, CoLM-Extinct and CoLM-Default, and CoLM-Snicar and CoLM-Extinct, respectively.

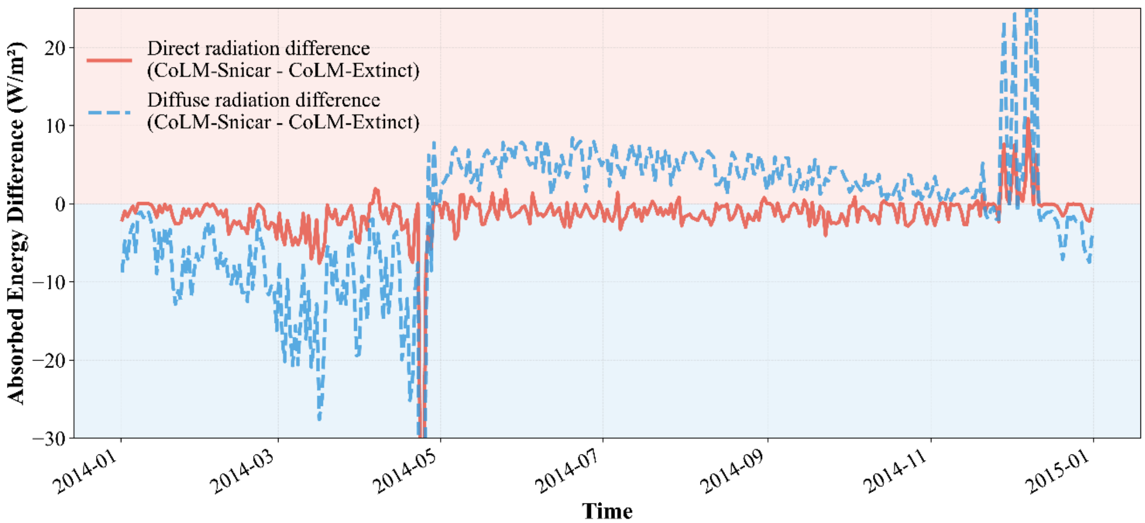

Figure S4. Differences in column-integrated absorbed direct and diffuse shortwave radiation between CoLM-Snicar and CoLM-Extinct during the open-water season of 2014 in Harp. Positive values indicate larger absorption in CoLM-Snicar.

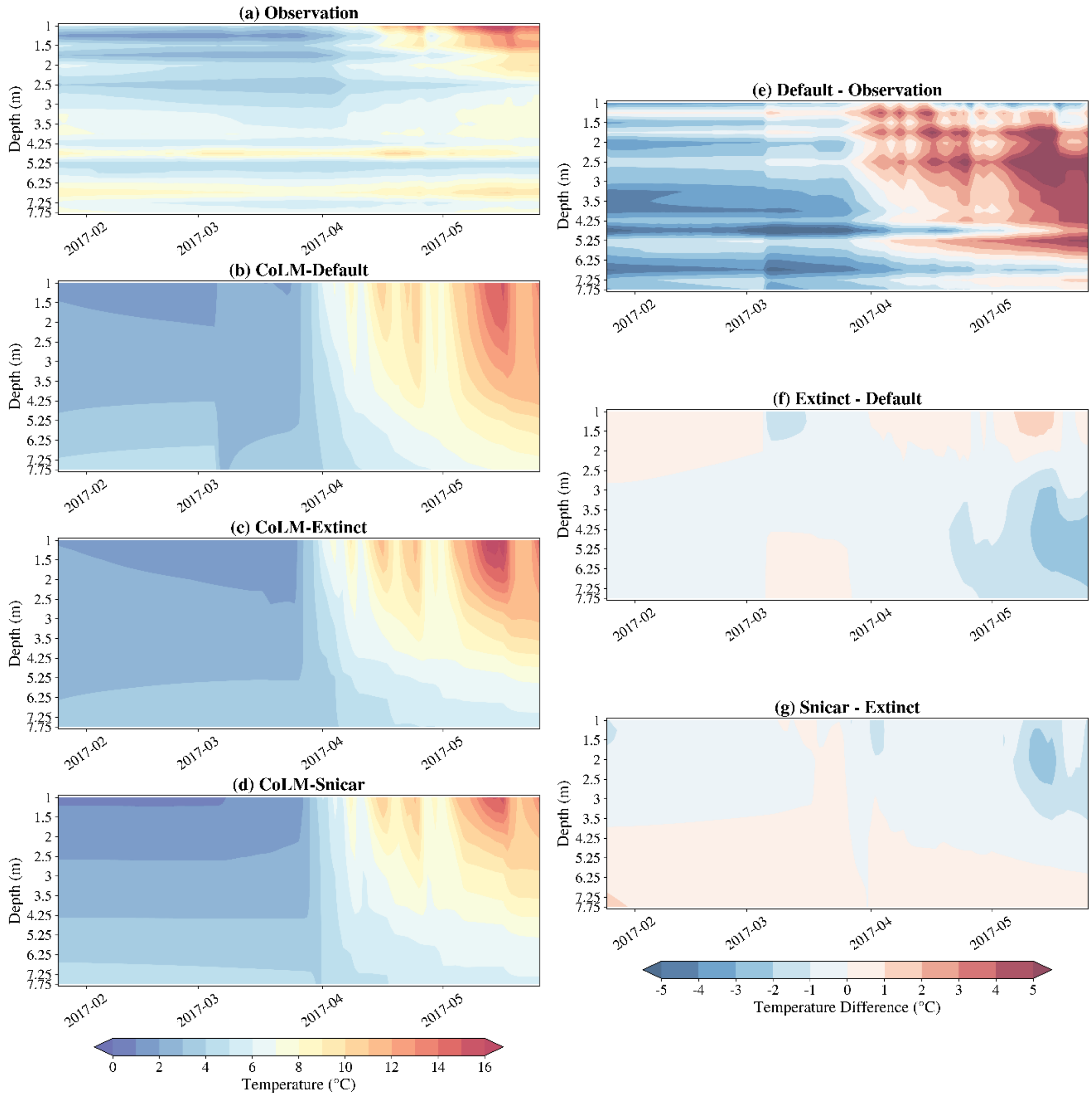

Figure S5. Observed and simulated water-temperature profiles in Lake Trout Bog. (a) Observations; (b-d) simulations from CoLM-Default, CoLM-Extinct, and CoLM-Snicar, respectively; (e-g) Simulated differences between CoLM-Default and observations, CoLM-Extinct and CoLM-Default, and CoLM-Snicar and CoLM-Extinct, respectively.

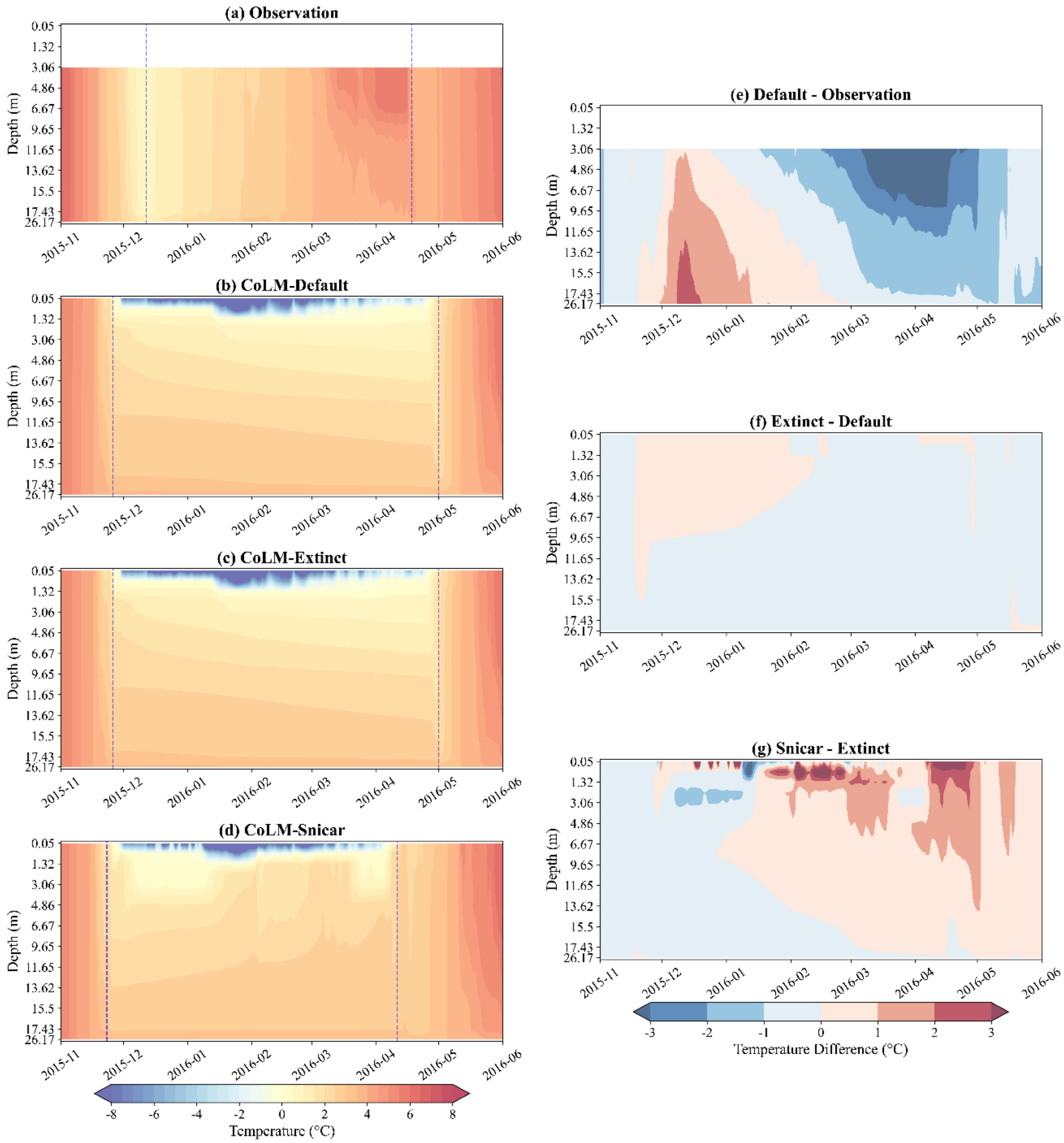

Figure S6. Observed and simulated water-temperature profiles in Lake Ngoring. (a) Observations; (b-d) simulations from CoLM-Default, CoLM-Extinct, and CoLM-Snicar, respectively; (e-g) Simulated differences between CoLM-Default and observations, CoLM-Extinct and CoLM-Default, and CoLM-Snicar and CoLM-Extinct, respectively. The dashed lines denote the freeze-up and break-up dates of lake ice.

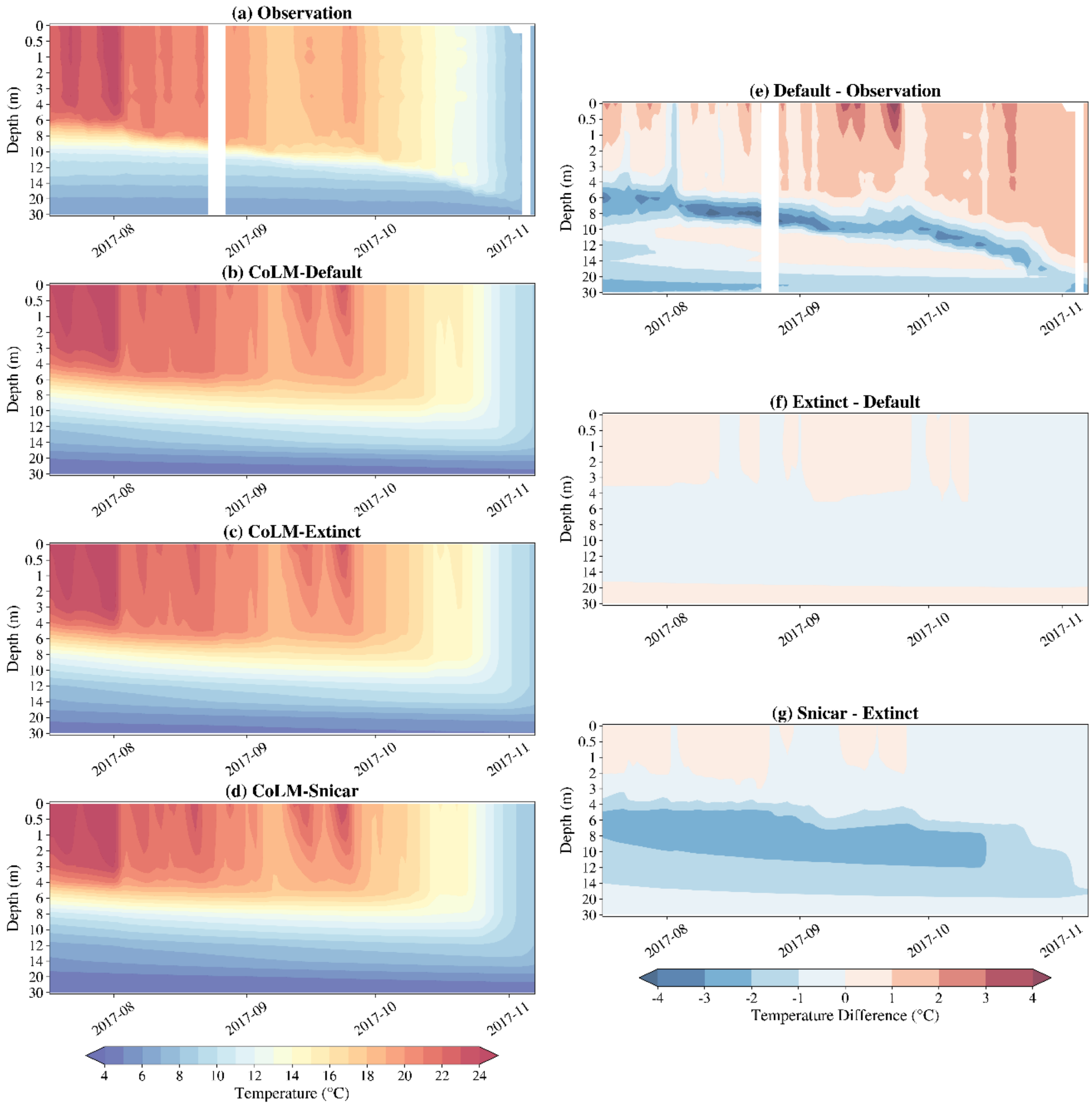

Figure S7. Observed and simulated water-temperature profiles in Lake Trout. (a) Observations; (b-d) simulations from CoLM-Default, CoLM-Extinct, and CoLM-Snicar, respectively; (e-g) Simulated differences between CoLM-Default and observations, CoLM-Extinct and CoLM-Default, and CoLM-Snicar and CoLM-Extinct, respectively.

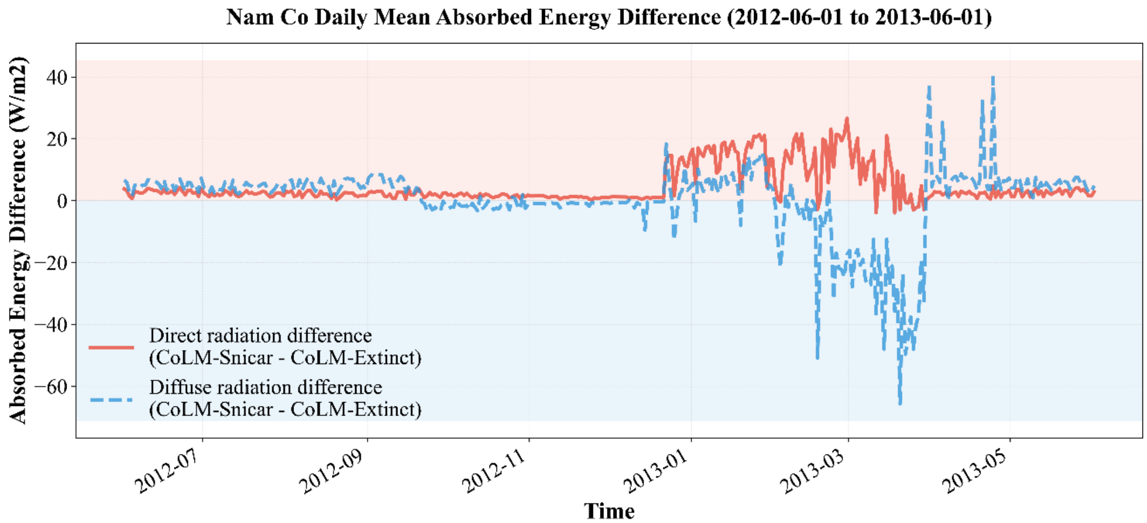

Figure S8. Differences in column-integrated absorbed direct and diffuse shortwave radiation between CoLM-Snicar and CoLM-Extinct during the open-water season of 2012.06-2013.06 in Nam Co. Positive values indicate larger absorption in CoLM-Snicar.

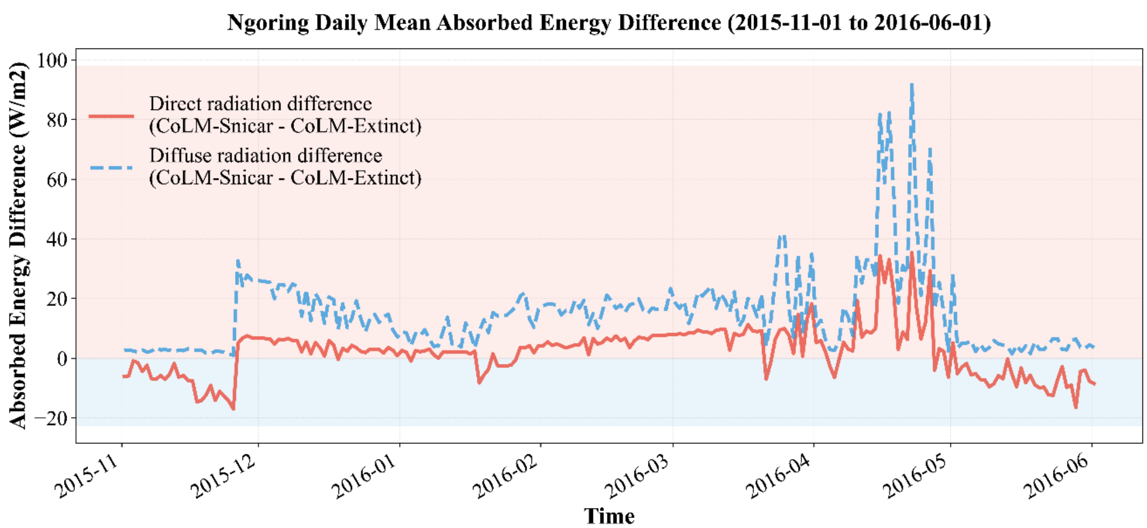

Figure S9. Differences in column-integrated absorbed direct and diffuse shortwave radiation between CoLM-Snicar and CoLM-Extinct during the open-water season of 2015.11-2016.06 in Ngoring. Positive values indicate larger absorption in CoLM-Snicar.

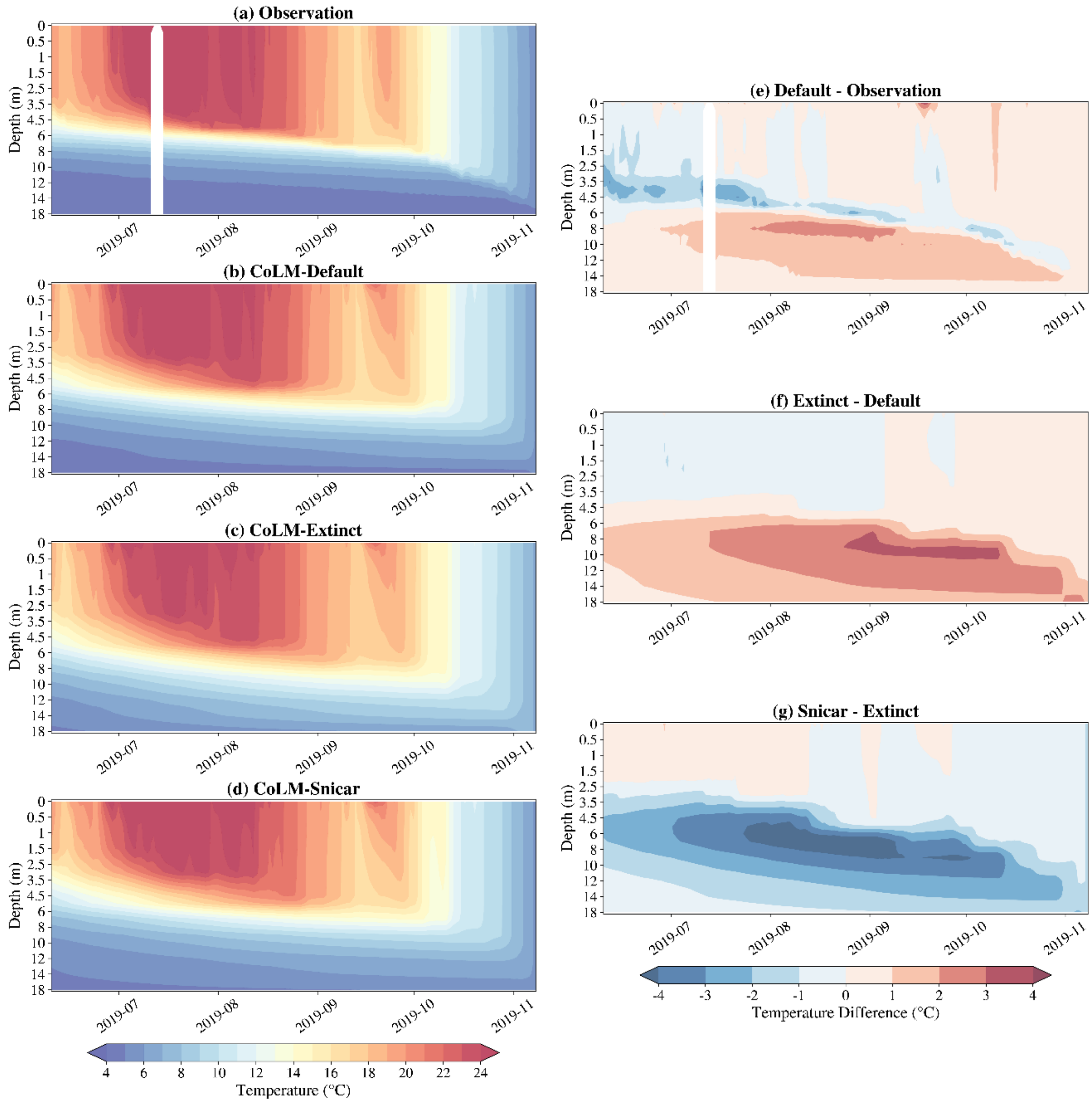

Figure S10. Observed and simulated water-temperature profiles in Lake Sparkling. (a) Observations; (b-d) simulations from CoLM-Default, CoLM-Extinct, and CoLM-Snicar, respectively; (e-g) Simulated differences between CoLM-Default and observations, CoLM-Extinct and CoLM-Default, and CoLM-Snicar and CoLM-Extinct, respectively.

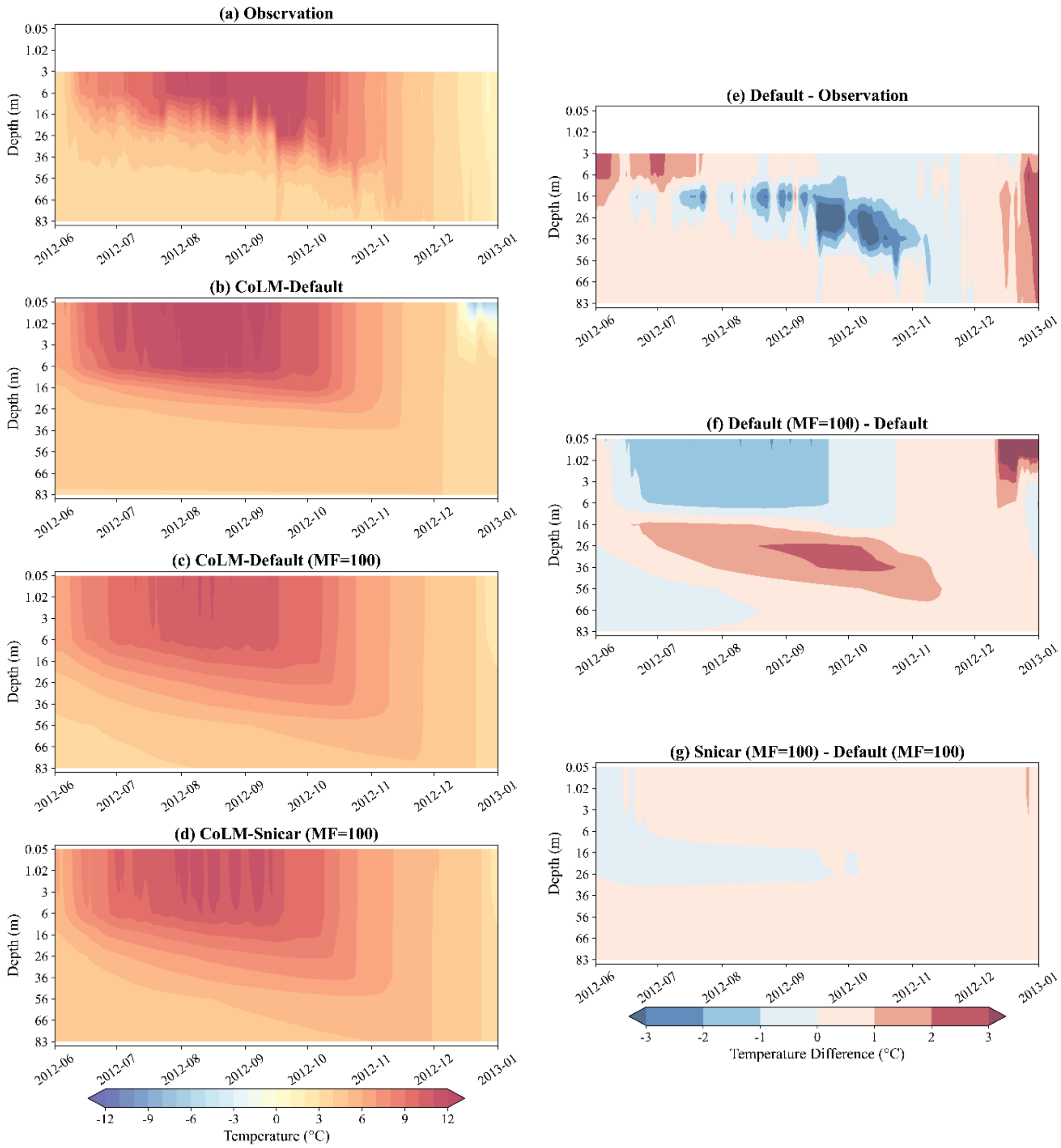

Figure S11. Sensitivity of simulated water-temperature profiles in Lake Nam Co to a 100-fold amplification of the vertical mixing coefficient (MF = 100). (a) Observations. (b–d) Simulations from CoLM-Default, CoLM-Default with the vertical mixing coefficient amplified by a factor of 100, and CoLM-Snicar with the same 100-fold amplification of the vertical mixing coefficient, respectively. (e–g) Simulated temperature differences: (e) CoLM-Default minus observations; (f) CoLM-Default with 100-fold enhanced vertical mixing minus CoLM-Default; and (g) CoLM-Snicar with 100-fold enhanced vertical mixing minus CoLM-Default with 100-fold enhanced vertical mixing. MF denotes the multiplier applied to the vertical mixing coefficient. Positive values indicate warmer temperatures in the first configuration named in each difference. Note that the light extinction coefficient is kept at its default value throughout this sensitivity test; only the vertical mixing coefficient is varied.

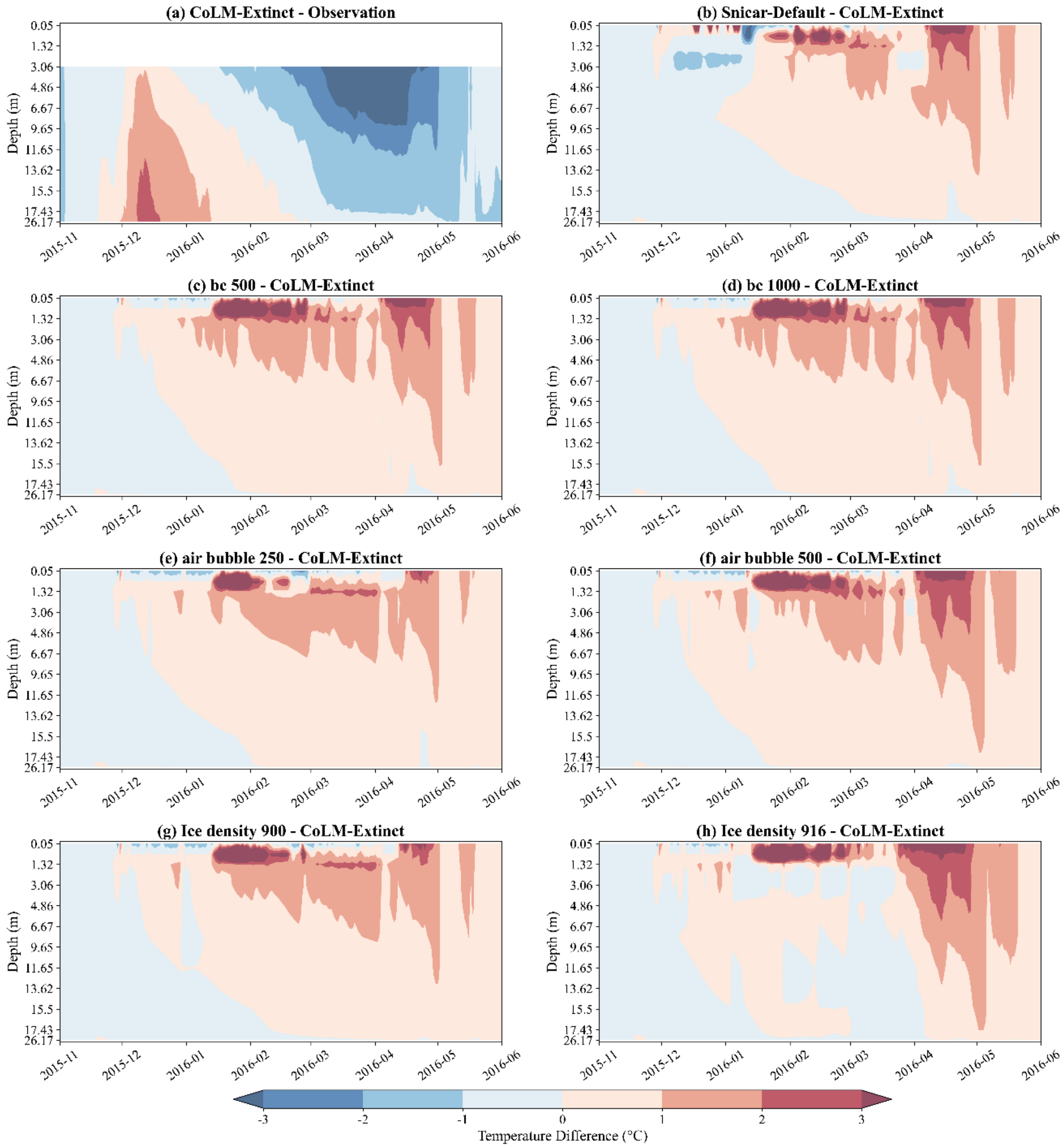

Figure S12. Sensitivity of simulated water-column temperature differences to SNICAR-ADv5 input parameters in Ngoring Lake. (a) Temperature difference between CoLM-Extinct and observations, while (b–h) Differences between SNICAR-based sensitivity experiments and CoLM-Extinct. The SNICAR-default experiment uses an ice density of 910 kg/m^3, an air-bubble radius of 750 μm, and a black carbon concentration of 0.

Table S1. Single Scattering Albedo (ω) of light-absorbing aerosols in the snowpack. Bands 1–5 correspond to wavelength ranges of 0.3-0.7, 0.7-1.0, 1.0-1.2, 1.2-1.5, and 1.5-5 µm.

Type	Band 1	Band 2	Band 3	Band 4	Band 5
Hydrophilic Black Carbon	0.516	0.434	0.346	0.276	0.139
Hydrophobic Black Carbon	0.288	0.187	0.123	0.089	0.040
Hydrophilic Organic Carbon	0.997	0.994	0.990	0.987	0.951
Hydrophobic Organic Carbon	0.963	0.921	0.860	0.814	0.744
Dust 1	0.979	0.994	0.993	0.993	0.953
Dust 2	0.944	0.984	0.989	0.992	0.983
Dust 3	0.904	0.965	0.969	0.973	0.978
Dust 4	0.850	0.940	0.948	0.953	0.955

Table S2. Mass Extinction Coefficient (τ) of light-absorbing aerosols in the snowpack (m^2/kg)

Type	Band 1	Band 2	Band 3	Band 4	Band 5
Hydrophilic Black Carbon	25369	12520	7739	5744	3527
Hydrophobic Black Carbon	11398	5923	4040	3262	2224
Hydrophilic Organic Carbon	37774	22112	14719	10940	5441
Hydrophobic Organic Carbon	3289	1486	872	606	248
Dust 1	2687	2420	1628	1138	466
Dust 2	841	987	1184	1267	993
Dust 3	388	419	400	397	503
Dust 4	197	203	208	205	229

Table S3. Asymmetry Factor (g) of light-absorbing aerosols in the snowpack

Type	Band 1	Band 2	Band 3	Band 4	Band 5
Hydrophilic Black Carbon	0.52	0.34	0.24	0.19	0.10
Hydrophobic Black Carbon	0.35	0.21	0.15	0.11	0.06
Hydrophilic Organic Carbon	0.77	0.75	0.72	0.70	0.64
Hydrophobic Organic Carbon	0.62	0.57	0.54	0.51	0.44
Dust 1	0.69	0.72	0.67	0.61	0.44
Dust 2	0.70	0.65	0.70	0.72	0.70
Dust 3	0.79	0.75	0.68	0.63	0.67
Dust 4	0.83	0.79	0.77	0.76	0.73